EUROFUSION WPHCD-PR(16) 16772

U Kurutz et al.

Investigations on Cs-free alternatives for negative ion formation

Preprint of Paper to be submitted for publication in
Plasma Physics and Controlled Fusion

This work has been carried out within the framework of the EUROfusion Consortium and has received funding from the Euratom research and training programme 2014-2018 under grant agreement No 633053. The views and opinions expressed herein do not necessarily reflect those of the European Commission.

Investigations on Cs-free alternatives for negative ion formation in a low pressure hydrogen discharge at ion source relevant parameters

U. Kurutz[1,2], R. Friedl[2], U. Fantz[1,2]

[1] Max-Planck-Institut für Plasmaphysik, Boltzmannstr. 2, 85748 Garching, Germany
[2] AG Experimentelle Plasmaphysik, Universität Augsburg, 86135 Augsburg, Germany

E-mail: uwe.kurutz@ipp.mpg.de

September 2016

Abstract. Caesium (Cs) is applied in high power negative hydrogen ion sources to reduce a converter surface's work function and thus enabling an efficient negative ion surface formation. Inherent drawbacks with the usage of this reactive alkali metal motivate the search for Cs-free alternative materials for neutral beam injection systems in fusion research. In view of a future DEMOnstration power plant, a suitable material should provide a high negative ion formation efficiency and comply with the RAMI issues of the system: reliability, availability, maintainability, inspectability. Promising candidates, like low work function materials (molybdenum doped with lanthanum (MoLa) and LaB_6), as well as different non-doped and boron-doped diamond (BDD) samples were investigated in this context at identical and ion source relevant parameters at the laboratory experiment HOMER. Negative ion densities were measured above the samples by means of laser photodetachment and compared with two reference cases: pure negative ion volume formation with negative ion densities of about $1\times10^{15}\,\mathrm{m}^{-3}$ and the effect of H^- surface production using an in-situ caesiated stainless steel sample which yields 2.5 times higher densities. Compared to pure volume production, none of the diamond samples did exhibit a measurable increase in H^- densities, while showing clear indications of plasma-induced erosion. In contrast, both MoLa and LaB_6 produced systematically higher densities (MoLa: $\times1.60$; LaB_6: $\times1.43$). The difference to caesiation can be attributed to the higher work functions of MoLa and LaB_6 which are expected to be about 3 eV for both compared to 2.1 eV of a caesiated surface.

PACS numbers: 29.25.Ni, 34.35.+a, 52.25.Jm

Keywords: Negative hydrogen ions, Cs-free, NNBI
Submitted to: *Plasma Phys. Control. Fusion*

1. Introduction

Neutral beam injection (NBI) based on negative ions (NNBI) is going to be a key system for heating and current drive (H&CD) at the International Thermonuclear Experimental Reactor (ITER) as it combines high current drive efficiency with a high heating power [1]. Also for the next step fusion device - the demonstration reactor DEMO, which is currently in the conceptual design status - NNBI using deuterium is under discussion for being a main H&CD system [2].
The respective negative ion sources are required to provide high energy particle beams in the MeV range with current densities of 200-300 $\mathrm{A/m^2}$ at highly homogeneous beam cross sections of about $\sim\mathrm{m^2}$ with pulse lengths of one hour or more. To minimize negative ion loss rates and power loads in the extraction and acceleration stages, ion sources must be operated at a gas pressure as low as 0.3 Pa and the ratio of inevitably co-extracted electrons to negative ions needs to remain below unity.
Negative ions in such sources can be formed in the plasma volume of the low temperature H_2/D_2 discharge as well as on surfaces facing the plasma [3]. The underlying mechanisms are respectively sensitive to the bulk plasma parameters as well as to the particle energies and fluxes impinging onto the so-called converter surface, i.e. the plasma grid (PG) of the extraction system.
For systems like ITER NNBI, the demanded parameters can up to date only be fulfilled by ion sources based on particle conversion at a caesiated surface [4]. In such systems, e.g. the ITER prototype sources developed and operated at the IPP (Garching, Germany), electron and positive ion densities in front of the PG are about $10^{16} - 10^{17}\,\mathrm{m^{-3}}$ and electron temperatures range between 1-2 eV [5]. Positive ion and neutral atom temperatures are about 0.8 eV and respective particle fluxes are $\Gamma_{i+} \sim 10^{20} - 10^{21}\,\mathrm{m^{-2}s^{-1}}$ and $\Gamma_H \sim 10^{22}\,\mathrm{m^{-2}s^{-1}}$ [6, 7].
The application of Caesium (Cs) leads to a reduction of the PG's work function from about 4 to 2 eV [8, 9, 10], thus enabling an efficient negative ion formation by converting the impinging atomic and ionic hydrogen particles [9, 11, 12]: The negative ion current increases by a factor between 5 and 10 while the co-extracted electron current decreases by up to an order of magnitude [4, 5].
However, there are several drawbacks inherently coupled to the usage of Cs: its complex chemistry as well its adsorption and redistribution dynamics (especially during plasma phases) causes an inherent long-term behaviour which inevitably affects the reliability of the ion source. The reaction of Cs with residual impurities can result in spatially inhomogeneous deterioration of the low work function. To counteract continuous evaporation of fresh Cs is mandatory. The resulting Cs consumption and a migration of Cs into the accelerator stages, where it lowers the components high voltage holding capabilities, are crucial issues regarding NNBI operation. At present, careful Cs conditioning of the ion source is required to achieve and maintain a high source performance [13]. These issues challenge especially the RAMI requirements of a DEMO NNBI system, i.e. high reliability and availability combined with good maintainability and inspectability.
The drawbacks motivate the search for Cs-free alternative materials for efficient negative ion formation for the next generation NNBI systems beyond ITER. Such alternatives should lead to a comparable enhancement of the negative ion density like the application of Cs or, if a slightly lower enhancement is given, at least eliminate Cs-related drawbacks.
In literature numerous investigations in the context of negative hydrogen ion formation are reported, using for example different refractory metals [14, 15, 16, 17], low work function materials [9, 18, 19] or carbon based materials like diamond [20, 21, 22]. However, partially inconsistent or even contrary results were obtained, or investigations were performed at conditions that do not apply for NNBI ion sources. A discussion about these investigations will be given below in section 2. Thus, in order to have a comparable set of measurements at identical and ion source relevant conditions, promising Cs-free materials are systematically investigated and directly compared. Therefore, a flexible laboratory experiment is used that provides plasma conditions with electron densities of 10^{16} to $10^{17}\,\mathrm{m^{-3}}$ and electron temperatures of about 1 eV. The materials effect on the H^- density is investigated also accounting for their impact on the bulk plasma, which affects the H^- related volume processes. This allows to assess the material's influence by direct H^- surface formation and/or indirect interference with the volume processes which determine an inherent present H^- background. It has to be noted that a materials effect on the negative ion density is throughout only detectable when it is at least comparable to the inherent, pure volume produced H^- background.
Results are furthermore compared to the effect of in-situ Cs application. Additionally, an insight into the material resistibilities against ion source plasma conditions is gained by using different surface analysing techniques.

2. Negative ion formation

2.1. Volume processes

Negative ions are formed in the plasma volume via dissociative attachment (DA), i.e. by the attachment of low energy electrons ($\sim$1 eV) to vibrationally excited

molecules. The formation rate is highly sensitive on the molecules vibrational quantum number and increases drastically in particular for $\nu \geq 5$ [3]

$$H_2(\nu \geq 5) + e \rightarrow H^- + H \quad . \tag{1}$$

As a consequence, negative ion volume formation requires a reasonable amount of vibrationally highly excited molecules. These precursors are formed in the plasma volume for example via the collision of energetic electrons ($\sim 20\,\mathrm{eV}$) with ground state molecules [23].
The H^- formation is balanced by the following destruction mechanisms:

- Electron Detachment:

  $$\mathrm{ED}: \quad H^- + e \rightarrow H + e + e \quad . \tag{2}$$

- Mutual neutralization:

  $$\mathrm{MN}: \quad H^- + H_x^+ \rightarrow H + H_x \quad (x = 1, 2, 3) \quad . \tag{3}$$

- (Non-)associative detachment:

  $$\text{non-AD}: \quad H^- + H \rightarrow H + H + e \quad , \text{and} \tag{4}$$
  $$\mathrm{AD}: \quad H^- + H \rightarrow H_2(X, \nu) + e \quad . \tag{5}$$

- Collisional Detachment:

  $$\mathrm{CD}: \quad H^- + H_2 \rightarrow H + H_2 + e \quad . \tag{6}$$

Consequently, low densities of electrons, positive ions, neutral atoms and hydrogen molecules are leading to low negative ion destruction rates. Furthermore, the electron detachment rate is decreased for low electron temperatures caused by the sensitivity of the corresponding rate coefficient on the electron temperature [24].
The contrasting parameters for efficient volume formation on the one hand and low destruction rates on the other hand are maintained by applying the tandem principle in the ion source design. Here, the plasma volume is separated into a heated driver region and a diffusive expansion region using a magnetic filter field for instance [25]. Within the heated driver region vibrationally excited molecules are produced which can diffuse into the non-heated expansion region where a lower mean electron energy is promoting the dissociative attachment process. Simultaneously, the low mean electron energy is correlated with a reduced H^- loss rate via ED.
Despite this possibility to optimize the volume formation, negative ion sources working in the volume regime still inherently require quite high electron and molecular hydrogen densities for high H^- production. Thus, they are typically operated at a pressure of about 1 Pa and extracted negative ion currents are commonly accompanied by high amounts of co-extracted electrons [3], so that the sources typically operate beyond the requirements of future NNBI systems.

2.2. Surface related processes

Materials can effect the negative ion density either by direct H^- surface formation as well as via an indirect effect that influences the negative ion related volume processes.

An indirect material induced effect can be given for example by the recombinative desorption process:

$$H + H + \text{wall} \rightarrow H_2(\nu) + \text{wall} \quad . \tag{7}$$

Thereby, the population distribution of vibrationally excited H_2, i.e. the precursor species for DA is catalytically affected by the surface material. This effect has been discussed for example by [26] in the context of different negative ion currents extracted form a volume based negative ion source ($p \leq 1\,\mathrm{Pa}$, $n_e \sim 10^{16} - 10^{17}\,\mathrm{m}^{-3}$, $T_e \sim 1\,\mathrm{eV}$). It is reported that covering the inner vessel walls by evaporation of tantalum filament material results in a more than about two times increased negative ion current ($\sim 0.7\,\mathrm{mA}$) compared to the case of using tungsten filaments ($\sim 0.3\,\mathrm{mA}$) together with an observed respectively different vibrational population distribution [26].
Another material induced effect on the volume processes is reported by [14]. Depending on the metal liners used within their arc discharge ($p = 0.2\,\mathrm{Pa}$, $n_e \sim 5 \times 10^{16}\,\mathrm{m}^{-3}$, $T_e \sim 0.5\,\mathrm{eV}$)also different H^- currents are observed. They correlated this to different H^- ED destruction rates caused by different amounts of high energetic electrons being injected by present potential differences from materials with different secondary electron emission coefficients into the bulk plasma in their discharge.
This is an example for different material related results obtained by different groups in filament driven setups: in one experiment the negative ion current was reduced by about 20 % when using tantalum liners instead of tungsten liners ([14]), whereas by [26] the negative ion current was increased when using tantalum instead of tungsten.

Direct negative ion formation at a surface proceeds by atomic or ionic particle conversion. The process basically relies on the transition of electrons from occupied states within the solid into the energy levels of an atomic hydrogen particle being in the solid's vicinity. The surface formation is thereby sensitive on the energetic structure of the solid (binding energy of electrons, present band gaps and surface states, ...) as well as on the position of the hydrogen particle's affinity level relative to the level of occupied states within the solid [27]. Since atomic and/or ionic hydrogen particles are converted, the formation rate is furthermore sensitive on the incoming atomic

and/or ionic hydrogen flux as well on the particle energies. Direct negative ion formation at different metal surfaces has been intensively studied in the past (see e.g. [28, 29, 11, 12]). It was found, that negative ions are formed via resonant charge transfer with a probability depending on the materials work function, which is the reason for applying Cs in present ion sources, since it has the lowest work function at room temperature (2.1 eV) of all applicable metals.
Quite recently, direct negative ion formation also was observed on diamond materials in particle scattering experiments [20, 30, 31] and in a hydrogen plasma discharge [21, 22]. An absolute negative ion yield of up to 5.5 % was measured for instance by [20] when scattering H_2^+ ions with particle energies of more than 200 eV.
In the low density hydrogen discharge ($p \leq 2$ Pa, $n_e \sim 10^{13}$ to 10^{14} m^{-3}, $T_e \leq 5$ eV [32]) investigated by [21, 22] the bombardment of different boron-doped-diamond (BDD) and non-doped diamonds with positive ions of more than 40 eV resulted in an enhanced negative ion yield in relation to all other investigated carbon based materials. However, within these investigations no absolute negative ion yields were measured, nor results were compared to Cs application.
In contrast to metals, the underlying formation process at diamond (work function of about 4 eV [33]) is not known at present. It is discussed for example by [30, 22] that H^- formation could be correlated with the characteristic of diamond having a low positive or even a negative electron affinity, a feature which is known to effect the possibility of emitting electrons from the solid state into vacuum [34].

3. Experimental setup

Measurements were performed at the flexible laboratory experiment HOMER (HOMogeneous Electron cyclotron Resonance plasma) which design allows for cw operation. A schematic of the ECR-experiment is shown in figure **??** (a) and a description of the setup can be found for instance in [35]. Briefly, the plasma is formed in a cylindrical vacuum chamber of 31 cm height and 7.5 cm radius, manufactured of stainless steel. The microwave, with a maximal power output of 1 kW, is transmitted through a borosilicate window from the top site of the vessel. A magnetic field of 87.5 mT, needed for resonant electron cyclotron heating, is generated homogeneously within the vessel volume by two water cooled solenoids located at the top and the bottom of the vacuum vessel. The vacuum pumps maintain a gas pressure of 0.3 Pa in hydrogen at a gas flow of 9 sccm.
Instead of using a magnetic filter field for applying the tandem principle, i.e. dividing the plasma volume into a heated driver and a non-heated, diffusive downstream region, HOMER is equipped with a meshed grid [36]. This method has the advantage, that no additional magnetic fields are required which interfere with the already present magnetic field of the ECR setup.
At HOMER vibrationally excited hydrogen molecules and hydrogen atoms are formed in the heated driver region of 2.1 l and diffuse through the stainless steel made meshed grid (mesh size ≈ 1 mm^2) into the diffusive downstream region. Here the distinct material samples are placed. The grid is located at a height of 19 cm relative to the bottom plate, electrically insulated against the grounded vessel walls. Material samples are placed in the diffusive downstream region onto a horizontally oriented mounting platform of 6×8.5 cm^2 in a distance of 4.5 cm to the meshed gird (see figure 1). The stainless steel made mounting platform is electrically and thermally insulated via a ceramic coupling and the sample holder bias can be modified relative to the grounded walls or the meshed grid for affecting the energy of charged particles which impinge onto the samples. The sample temperature is monitored via a thermocouple installed at the top side of the sample holder and samples can be heated in plasma and vacuum up to 450 °C.

3.1. Diagnostics

A quantification of the negative hydrogen ion density is performed by means of laser photodetachment [37]. A Nd:YAG laser is used that provides laser pulses of maximal 50 mJ energy per pulse at the first fundamental ($\lambda = 1064$ nm). The laser beam is coaxially aligned onto a Langmuir probe tip (100 μm diameter, tungsten) which is positioned parallel and centred to the sample surface (see figure 1 (b)). At the location of the probe tip the laser beam has a diameter of 6 mm. By default, the Langmuir probe is distanced 2 cm below the meshed grid and accordingly 2.5 cm above the respective sample surface.
The density of negative ions is measured locally, but relatively to the electron density (n_{H-}/n_e). Absolute H^- densities are subsequently deduced via quasi-neutrality using the positive ion density due to the present magnetic field. The latter density is obtained from the positive ion saturation branch of the Langmuir probe characteristic via OML theory [38]. The applied laser photodetachment diagnostic at HOMER has been successfully benchmarked against cavity ring-down spectroscopy (CRDS) [39], an independent and highly reliable diagnostic for the negative ion density. Additionally to the measurement of the negative ion density, bulk plasma parameters like the electron energy distribution function (EEDF) as well as the plasma and floating potentials

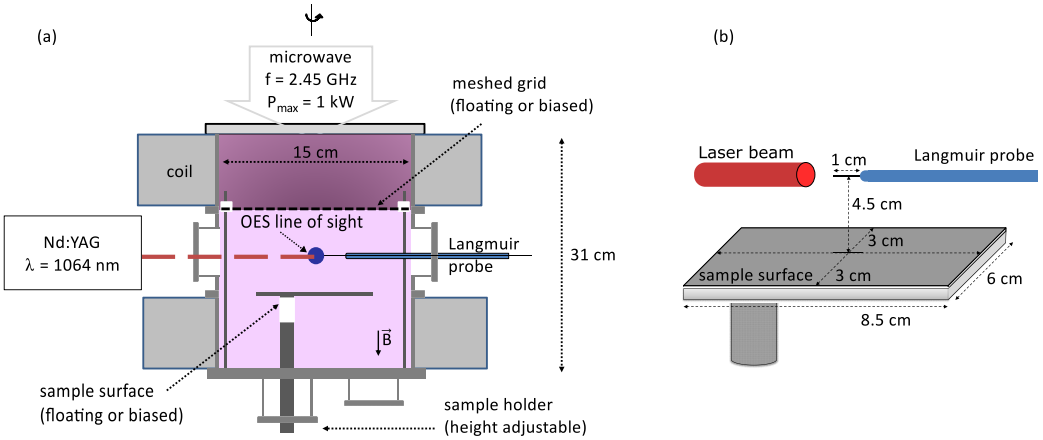

Figure 1. (*a*) Schematic drawing of the experimental setup HOMER (front view). (*b*) Sketch for illustrating the relative orientation of the Langmuir probe tip and the sample surface.

are determined via the Langmuir probe system. Furthermore, optical emission spectroscopy (OES) is used to obtain the atomic to molecular hydrogen density ratio as well as the vibrational, the gas and the atomic hydrogen temperature by analysing the emission of the Balmer transition and of the vibrational bands of the Fulcher transition after [40, 41]. The line of sight is at the same hight like the Langmuir probe tip but perpendicular orientated to the tip (see figure 1). The spectroscopic system is intensity calibrated with a Gaussian apparatus profile having a FWHM of 23 pm at 400 nm and 17 pm at 850 nm.

3.2. Modelling of the H⁻ volume processes

Using the determined parameters, the volume processes are modelled in a 0-dimensional approach by means of the solver YACORA [6, 39]. The model allows for calculating the steady-state H^- density by balancing the formation via dissociative attachment against the H^- destruction via associative and non-associative detachment ((non)AD), electron detachment (ED), collisional detachment (CD) and mutual neutralization (MN):

$$\sum_{\nu} n_{\mathrm{H_2(X},\nu)} n_{\mathrm{e}} X^{\nu}_{\mathrm{DA}}(\mathrm{EEDF}) = \\ = n_{\mathrm{H^-}}(n_{\mathrm{e}} X_{\mathrm{ED}}(\mathrm{EEDF}) + n_{\mathrm{H}} X_{\mathrm{(non)AD}}(T_{\mathrm{H}}, T_{\mathrm{H^-}}) + \\ + n_{\mathrm{H_2}} X_{\mathrm{CD}}(T_{\mathrm{H_2}}, T_{\mathrm{H^-}}) + \sum_{\mathrm{x}=1,2,3} n_{\mathrm{H_x^+}} X_{\mathrm{MN}}(T_{\mathrm{H_x^+}}, T_{\mathrm{H^-}})) \quad . \tag{8}$$

Here, $n_{\mathrm{H_2(X},\nu)}$, n_{H} denote the densities of the different vibrationally excited molecules in ground state as well as the atomic hydrogen density. The electron as well as the negative and different positive ion densities (H^+, H_2^+, H_3^+) are represented by n_{e}, $n_{\mathrm{H^-}}$, $n_{\mathrm{H_x^+}}$, respectively. The rate coefficients X are calculated for the different temperatures of molecular hydrogen ($T_{\mathrm{H_2}}$), atomic hydrogen (T_{H}) as well as for different positive ion species temperatures ($T_{\mathrm{H_x^+}}$) and H^- temperatures ($T_{\mathrm{H^-}}$) or an experimentally determined EEDF, respectively on bases of cross section data compiled in [42]. As described in [39], the impact of the experiment's design after the tandem principle is accounted for by describing the vibrational population distribution of H_2 via a two-temperature Boltzmann distribution, characterized by the two temperatures $T_{\mathrm{vib}}^{\mathrm{low}}$ and $T_{\mathrm{vib}}^{\mathrm{high}}$. The population distribution of the low lying vibrational states ($\nu \leq 3$) is described by $T_{\mathrm{vib}}^{\mathrm{low}}$, experimentally determinable via OES [40]. The population distribution of the vibrationally highly excited states is outside the accessible range for the applied diagnostic system. Hence, modelling of $n_{\mathrm{H^-}}$ is performed using measured plasma parameters together with $T_{\mathrm{vib}}^{\mathrm{high}}$ as a free parameter which allows to adapt the modelled to the measured H^- density.

3.3. Measurement procedure

Cs-free materials were investigated for comparability reasons throughout at constant plasma conditions, i.e. at 0.3 Pa gas pressure and 300 W discharge power. Their effect on the H^- density was studied as a function of applied sample bias for studying the influence of the energy and the flux of impinging charged particles as well as of the energy of negative ions leaving the surfaces. However, due to the experimental design, a variation of the sample bias (experimentally accessible range between -30 and +20 V relative to the grounded vessel walls) also affects the complex interplay of the different potentials in the diffusive downstream region, the driver region and the meshed grid.
To account for a possibly resulting influence on the inherent H^- volume processes and in order to assess the Cs-free materials influence on the H^- density, measurements were always compared to pure volume

formation reference measurements. Therefore, a stainless steel dummy sample was used, providing an insight into the evolution of the H^- background at comparable plasma conditions and also at comparable potential field geometry like in case of the studies on Cs-free materials. Measurements were furthermore compared to the effect of in-situ caesiation of a stainless steel sample, providing a second reference case. Therefore, Cs was applied via evaporation, using an alloy Cs dispenser purchased from [43]. The dispenser was installed in a short distance to sample with the opening towards the sample in order to keep source contamination by Cs low. Furthermore, the vessel has been carefully cleaned afterwards and a steel sample was tested again to exclude any remaining Cs effect.

The introduction of Cs onto the floating stainless steel sample results in an immediate increment of the H^- density by up to a factor of 2.5. The difference to the enhancing effect of Cs known from larger negative ion sources like the IPP test stand Batman [4] (factor 5 to 10) is dominantly attributed to the differing particle fluxes onto the respective surfaces. While at HOMER Γ_H is about $5\times10^{21}\,m^{-2}s^{-1}$ and Γ_{i+} about $1\times10^{20}\,m^{-2}s^{-1}$, respective fluxes of up to $3\times10^{22}\,m^{-2}s^{-1}$ and up to $7\times10^{20}\,m^{-2}s^{-1}$ are present at Batman [44].

3.4. Investigated Cs-free materials

Measurements were focused on materials where a direct H^- surface formation is expected or reported (see section 2.2.

In case of the low work function materials bulk samples of molybdenum doped with 0.7 % lanthanum (MoLa) and LaB_6 were investigated. According to [45] and [46] a work function of down to 2.6 eV is given in both cases for temperatures of above 1000 °C.

The MoLa and the LaB_6 samples were respectively purchased from the commercial distributors [47] and [48], respectively. They had a polycrystalline material structure caused by manufacturing via press sintering. Since the underlying mechanism for negative ion formation at diamond including a potential sensitivity on features like the grain size, the crystallinity or the doping level is not known at present, a variety of different non-doped and boron-doped diamond (BDD) samples were used. In table 1 the characteristics, deposition methods and suppliers of the two investigated non-doped (in the following labelled with diamond#1 and diamond#2) and three BDD samples (in the following labelled with BDD#1, BDD#2 and BDD#3) can be found for completeness. The samples have either been deposited via microwave plasma assisted chemical vapour deposition (MPACVD), high-frequency chemical vapour deposition (HFCVD) or plasma enhanced chemical vapour deposition (PECVD).

4. Results and Discussion

4.1. Effect of sample bias variations on inherent H^- volume processes

In figure 2 the negative ion density as a function of sample bias for the stainless steel reference sample, i.e. of the effect on the inherent present volume processes is shown. Additionally, corresponding electron densities and the vibrational temperatures T_{vib}^{high} are depicted. The latter are deduced via modelling. In the bias range between -30 and -10 V n_{H^-} is minor influenced, whereas it increases from $7.5\times10^{14}\,m^{-3}$ to maximally $1.0\times10^{15}\,m^{-3}$ with increasing sample bias in the more positive bias range. In contrast, the electron density is virtually constant $1.2\times10^{16}\,m^{-3}$ within the error margins. Consequently, the relative negative ion density ratio n_{H^-}/n_e is between 6 and 10 %. According to the model, this H^- density is given for vibrational temperatures T_{vib}^{high} of between 10600 and 8400 K in the negative bias range and about 8400 K for all of the positive bias range. In contrast, the experimentally accessible vibrational temperature T_{vib}^{low} as well as the gas and the atomic hydrogen temperature (not shown here) are nearly unaffected by sample bias variations in the entire investigated range, being about 3500 K and 500 to 600 K, respectively.

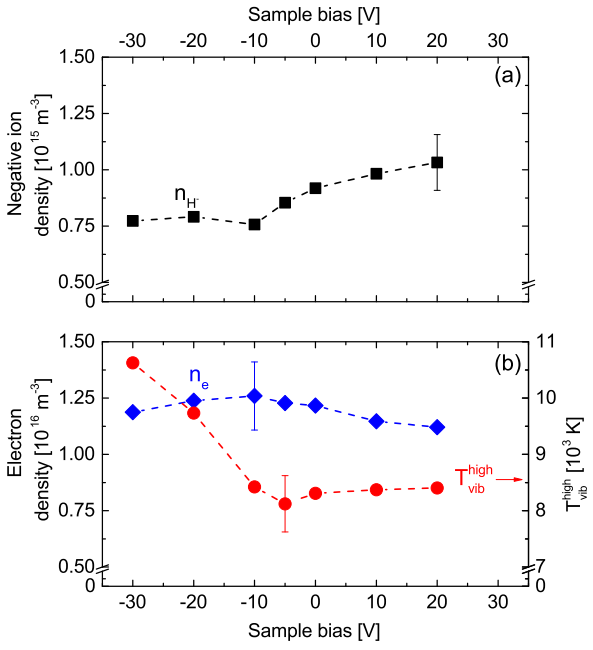

Figure 2. (a) Negative hydrogen ion density and (b) electron density as a function of sample bias for stainless steel sample.

A sample bias variation has a pronounced impact

Table 1. Overview of investigated diamond materials.

	diamond#1	**diamond#2**	**BDD#1**	**BDD#2**	**BDD#3**
Crystallinity	polycr.	epitaxial	polycr.	polycr.	polycr.
Sample size [cm^2]	34	4	31.4	51	20
Thickness of diamond layer [μm]	7.5×10^2	13	3	not specified	12
Average grain size [μm]	150	2.5	1.8	not specified	3
Substrate material	-	Si $\langle 0\,0\,1\rangle$	Si polycr.	Mo polycr.	Nb polycr.
Deposition method	MPACVD	MPACVD	PECVD	MPACVD	HFCVD
Boron doping level [$10^{18}\,m^{-3}$]	0	0	1.5	0.5	0.1
Supplier	[49]	[49]	[50, 51]	[52, 53]	[54]

on the EEDF, in particular in the negative bias range where electrons are repelled and an increasing positive ion flux has to be balanced (Maximal positive ion impinging energy ~10 eV). The left in figure 3 shows the corresponding trend of the mean electron energy. The values were deduced from the measured EEDFs which all showed a pronounced bi-Maxwellian character throughout the investigations. A changing mean electron energy directly affects the volume formation via DA as well as the H^- destruction via ED. Furthermore, this parameter influences the population of vibrationally excited H_2 states.

Regarding the H^- related destruction processes, a changing atomic to molecular hydrogen density ratio was observed during sample bias variations. This parameter is correlated with the H^- destruction via atomic hydrogen collisions ((non)AD). The evolution is shown on the right in figure 3 and ranges between 8 % and 10 %. (The depicted error bar accounts for the uncertainty of absolute value determination. The relative behaviour however is estimated to have a much lower error bar.)

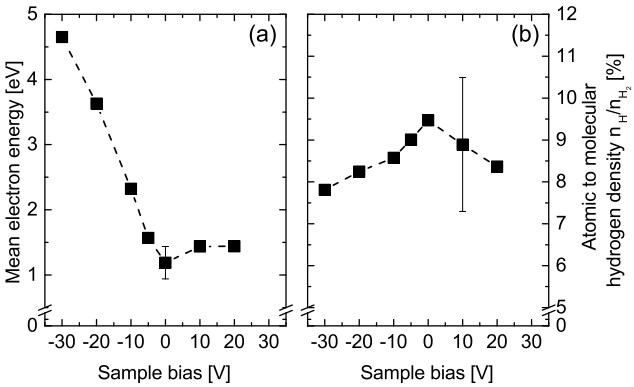

Figure 3. (a) Mean electron energy and (b) atomic to molecular hydrogen density ratio as a function of sample bias of the stainless steel sample.

The relevancy of the different destruction channels, analysed via the 0-dimensional model for n_{H^-}, shows that H^- destruction via atomic hydrogen and electron collisions represent the main destruction channels. In figure 4 the relative shares of the negative ion destruction channels are depicted. As can be seen, negative ions are predominantly (up to 50 %) destroyed in the negative bias range, via ED as a consequence of the high mean electron energies. In the positive and moderate negative bias range (-10 to +20 V), atomic hydrogen collisions become of highest relevance for the H^- destruction, contributing with a share of at least 66 %. The analyses show that varying the sample bias

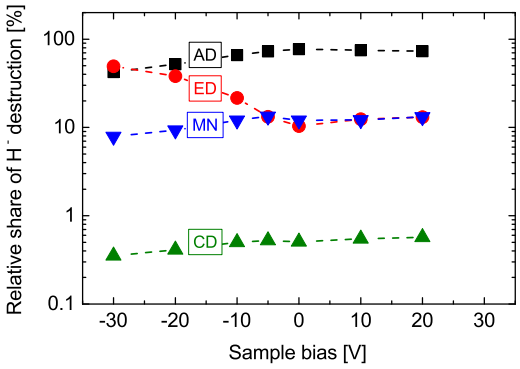

Figure 4. Relative share of the different H^- destruction channels as a function of sample bias for stainless steel sample determined via 0-dimensional model. The destruction by atomic hydrogen collisions is presented as a combined channel labelled with 'AD'.

directly impacts the background negative ion density determined by changes of both, negative ion volume formation and destruction.

4.2. Bias variations on low work function materials

In figure 5 the negative ion density is shown as a function of sample bias for the low work function materials MoLa and LaB_6 together with the respective stainless steel reference measurements. Corresponding measurements regarding isotopic differences can be found in

[55]. In order to maintain a reduced work function e.g. by removing volatile impurities on the surface of the MoLa and the LaB_6 samples, the sample temperatures were respectively set to the experimentally maximal achievable temperature of 450 °C.
Both low work function materials resulted relative to the reference case in a systematic increased n_{H^-}, most pronounced in the bias range between -10 and +20 V (15 to 60 % for MoLa and 25 to 43 % for LaB_6). For a negative bias of more than -20 V, the observed difference clearly diminishes. The H^- densities are in the same order of magnitude for all investigated materials and basically show the same trends for sample bias variations. This implies that for all samples a significant impact on the measured n_{H^-} is determined by changes of the H^- background, i.e. the inherent volume processes.

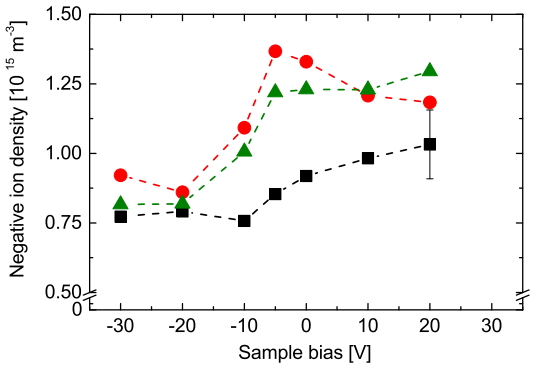

Figure 5. Negative ion density as a function of sample bias for heated MoLa and LaB_6 (450 °C) together with stainless steel reference measurements.

Experimentally deduced plasma parameters related to the H^- volume processes nearly did not show a dependency on the installed sample material, i.e. virtually the same electron densities, vibrational temperatures T_{vib}^{low} and mean electron energies were measured. Also the atomic to molecular hydrogen density ratio was within its error margins comparable to that determined during the stainless steel measurements, but showed a slightly different evolution, i.e. nearly monotonously increasing with increasing bias instead of being peaked (see figure 6).

It has to be noted that a changing atomic hydrogen density affects in case of the low work function materials both, the H^- destruction as well as the H^- surface production. The latter influence is caused by the coupling to the atomic particle flux ($\Gamma_H \approx 2.0\times10^{21}\,m^{-2}s^{-1}$). Like in case of the stainless steel sample, T_H was nearly constant about 500 to 600 K. Hence, the increment of the atomic hydrogen density

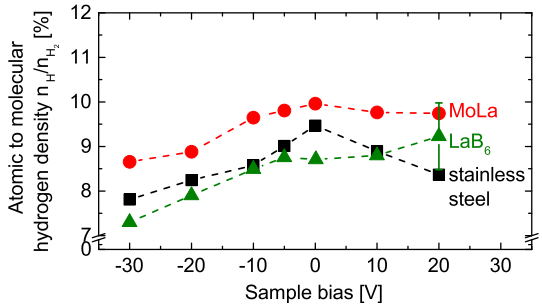

Figure 6. Atomic to molecular hydrogen density ratio as a function of sample bias for heated MoLa and LaB_6 (450 °C) together with stainless steel reference measurements.

with increasing bias leads to an enhanced atomic hydrogen flux onto the surfaces. Accordingly, the measured difference in n_{H^-} between the low work function materials and stainless steel implies, especially in the positive bias range, the presence of an additional source for negative ions coming from the surface. In the negative bias range however the lower atomic hydrogen flux seems not to be sufficient to enhance the H^- density in a measurable amount so that H^- surface production is masked by changing volume processes.
Regarding the influence of the positive ion flux (correlated with the positive ion energy), the measurements furthermore imply that changing this latter flux to maximally $1.5\times10^{20}\,m^{-2}s^{-1}$ with particle energies up to about 10 eV minor impacts the H^- surface formation, at least below the detection limit. This may be correlated either with the energy or might be a consequence of the generally low positive ion flux which is lower by an order of magnitude relative to the atomic hydrogen flux.

4.3. Investigations on diamond materials

Measurements with diamond materials were performed with and without additional heating. The performed campaigns with additional heating were motivated by the results reported by [21, 22]: the authors measured an increment of the determined relative H^- yield in their low density discharge by about an factor of three, when they heated their BDD sample to about 400 °C. In figure 7 (a) the effect on n_{H^-} is shown for not actively heated samples (the sample temperature did not exceed 160 °C) and in figure 7 (b) for actively heated BDD samples ($T_{smpl} \approx 450$ °C).

In contrast to the low work function materials, none of the diamond samples resulted in a measurable enhancement of the negative ion density exceeding the pure volume production. Independent of applied

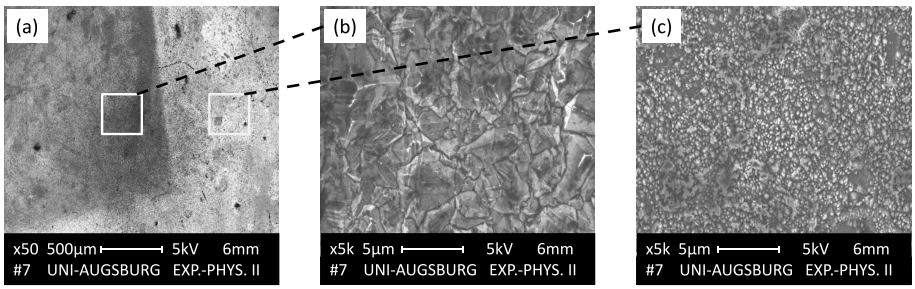

Figure 8. SEM pictures of BDD#3. (a) Section showing pristine (dark) and plasma exposed areas (lighter). (b) Zoomed-in to pristine area. (c) Zoomed-in to plasma exposed area.

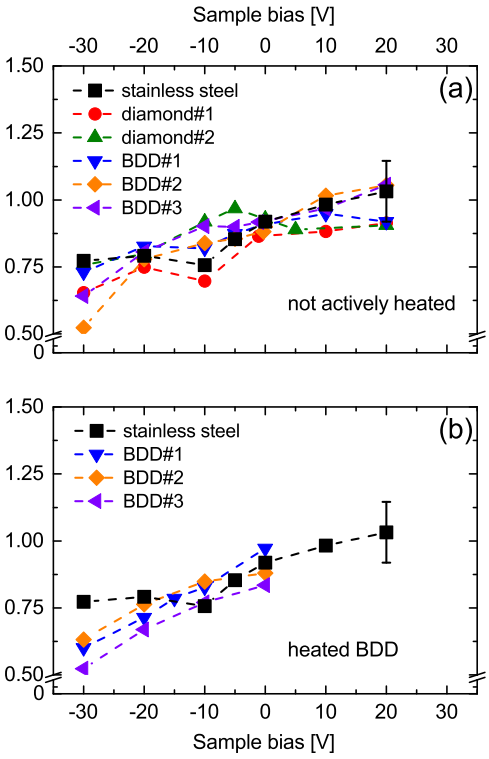

Figure 7. Negative ion density as a function of sample bias for (a) not actively heated diamond materials ($T_{\mathrm{smpl}} \leq 160\,^{\circ}\mathrm{C}$) and (b) heated BDD samples ($T_{\mathrm{smpl}} \approx 450\,^{\circ}\mathrm{C}$) in comparison with stainless steel used as reference.

bias and in case of BDD also independent of temperature virtually the same negative ion densities like with the stainless steel reference sample were observed. However, all diamond materials significantly affected the bulk plasma throughout the investigations: compared to stainless steel the atomic hydrogen density was reduced by up to 73 % and an at least 500 K higher vibrational temperature $T_{\mathrm{vib}}^{\mathrm{low}}$ was determined via OES, independent of the applied bias. Both effects should lead to an increased amount of H^- coming from the volume processes (higher production at simultaneously lower destruction rate). Thus, the absent enhancement of n_{H^-} may either be caused by unwanted collisions of vibrationally excited H_2 with carbon and/or hydrocarbons, adversely affecting the population of vibrationally highly excited states or by the presence of further unknown H^- destruction mechanisms e.g. by hydrocarbon collisions. However, although such mechanism can mask a potentially present H^- surface production, it has to be noted that the absent H^- enhancement together with the pronounced impact on the bulk plasma do not comply with the requirements of a Cs-free alternative converter material.

Furthermore, all investigated diamond samples showed clear signs of plasma induced erosion so that a reduced sample weight and a modified surface structure was given after plasma exposure times of maximally 10 h. The latter effect is shown in figure 8 exemplarily for the BDD#3 sample by means of SEM measurements. The visible darker section on the sample surface has been covered by a stainless steel mask to cancel out a direct plasma contact and represents the pristine surface structure. In contrast, the lighter surface section has been directly exposed to the hydrogen plasma. Respectively zoomed-in pictures are depicted in figure 8 (b) and (c). As can be seen, the polycrystalline, i.e. pristine surface structure (figure 8(b)) is clearly modified due to the plasma exposure (figure 8(c)), i.e. the plane texture is transformed into a structure of a higher surface roughness. This effect also was observed for the other diamond samples. Furthermore, for all diamond samples a reduced sample weight was measured after plasma exposure. The determined erosion rate was up to 1×10^{-3} g/h. The different results regarding measurements presented here and those reported by [21] and [22] may be correlated to the impinging positive ion energies or different volume processes in the respective experimental setups. By [21, 22] the negative ion formation was investigated during positive ion bombarding with energies $\geq$40 eV, whereas at HOMER the positive ion energy is like in NNBI ion sources below 10 eV. Hence, H^- formation at diamonds by positive ion bombardment seems to be

characterised by a certain threshold for the positive ion energy. Plasma conditions in both experimental setups are furthermore significantly differing. An electron density of more than $10^{16}\,\mathrm{m}^{-3}$ is given at HOMER for instance, while it is according to [32] between 10^{13} - $10^{14}\,\mathrm{m}^{-3}$ in the experimental setup used by [21, 22]. Thus, the negative ion background density determined by the volume processes is different or might even be negligible in case of the measurements performed by [21, 22] and thus not overcompensating H^- surface formation in contrast to HOMER. It has to be furthermore noted that [21, 22] did not measure absolute negative ion densities but rather variations in the relative negative ion yield using mass spectrometry. Thus, with respect to the different plasma conditions and applied diagnostics the possibility for a direct comparison of the results gained at HOMER and by [21, 22] is rather limited.

4.4. Comparison with a caesiated surface

In figure 9 the H^- density measured for different Cs-free materials is compared with the enhancement resulting from in-situ caesiation of a stainless steel sample. Depicted data include measurements performed with the low work function materials MoLa and LaB_6, the described different diamond materials, the stainless steel reference as well as the caesiated stainless steel sample (labelled as 'stainless steel + Cs'). Furthermore, measurements with a bulk tantalum and a bulk tungsten sample are shown as measured by [35]. All measurements were performed without the application of any sample bias at the same external parameters. Except for the low work function materials none of the samples were actively heated.

All investigated diamond materials as well as the bulk tantalum and tungsten sample resulted in a nearly identical negative ion densities like the stainless steel reference case.

An enhancing effect was only observed for the low work function materials MoLa and LaB_6. However, the enhancement is lower than in case of in-situ Cs application. This is probably attributed to their higher work functions. According to [45] and [46] both materials have a work functions of down to 2.6 eV when heated to above 1000 °C. However, due to the setup design the sample temperatures were not exceeding 450 °C, respectively. Since a materials work function is known to be generally temperature sensitive due to the amount of impurities contaminating, and therefore modifying the sample surface [10] a higher work function is expected. First preliminary investigations at another setup which provides similar conditions like at HOMER and allows for the measurement of the work function indicates that the respective work functions are about 3 eV. For comparison, at such conditions, work functions down to 2.1 eV have been reported for caesiated surfaces by [8].

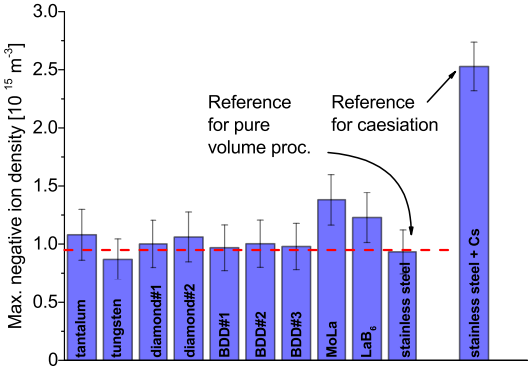

Figure 9. Maximal measured negative ion density for different materials at same external experimental conditions: measured in a distance of 2.5 cm to unbiased samples, at 0.3 Pa H_2 pressure and 300 W discharge power.

5. Summary and Conclusion

Different Cs-free materials for negative hydrogen ion formation have been investigated at parameters relevant for ion sources of future NNBI systems. Their effect was directly compared to the steady state n_{H^-} determined by pure H^- volume processes and to the effect of H^- surface formation at an in-situ caesiated surface using one distinct experimental setup. Among the investigated Cs-free materials neither any of the investigated diamond materials nor bulk samples made of tantalum nor tungsten resulted in an enhanced negative ion density relative to the pure volume reference case. Moreover, all diamond materials significantly influenced the bulk plasma and showed, already within plasma on times of 10 h, clear signs of plasma-induced erosion. This clearly contradicts a demanded long-term stability of a Cs-free alternative grid material in NNBI ion sources. Hence, these materials cannot be seen as alternatives to the application of Cs.

In contrast, both low work function materials MoLa and LaB_6 lead to a systematically increased negative ion density compared to the pure volume reference case. Measured negative ion densities furthermore exceeded those expected from modelling of the volume processes which indicates a direct H^- surface production. A difference of the maximal measured enhancement ($\times$ 1.60 in case of MoLa and $\times$ 1.43 in case of LaB_6) compared to the enhancement of in-situ caesiation ($\times$ 2.5) is attributed to their higher work functions. In both cases a work function of about 3 eV is expected according to first preliminary investigations compared to about 2.1 eV in case of Cs. Despite this

difference, further investigations are needed to evaluate the full potential of these materials, regarding for example whether the lower enhancement overcompensates the out-cancelled drawbacks linked to Cs evaporation, since for example bulk samples of MoLa or LaB_6 could be used.
Dedicated investigations regarding higher sample temperatures and the maximally extractable negative ion currents at simultaneously given co-extracted electron currents (a limiting factor for NNBI systems) would be required in a next step, in order to evaluate the potential of MoLa and LaB_6 for being Cs-free alternative converter materials in negative ion sources. Although well known that negative ion surface formation reduces the amount of electrons in the vicinity of the converter surface (see for instance [56]), the actual influence of these materials on the extracted currents have to be investigated directly at a negative ion source providing an extraction system.
Furthermore, the evolution of the respective work functions during plasma exposure should be investigated. In this context the stability as well as possibilities for maintaining minimal values of the work function as well as counteracting procedures for any unwanted deterioration are necessary.

Despite the lower enhancement, the results generally show that materials with inherent low work function can be seen as the most promising types of materials for being Cs-free alternatives in future NNBI ion sources like for DEMO. It is therefore recommended that further investigations should be focused on this type of materials.

Acknowledgments

The authors would like to thank Dr. M. Schreck (Augsburg University (Germany)) and Dr. G. Cartry (Aix-Marseilles University, CRNS, PIIM (France)) for the provision of diamond samples. This work has been carried out within the framework of the EUROfusion Consortium and has received funding from the Euratom research and training programme 2014-2018 under grant agreement No 633053. The views and opinions expressed herein do not necessarily reflect those of the European Commission.

[1] IAEA. ITER technical basis. ITER EDA documentation series 24, International Atomic Energy Agency, Vienna, 2002.

[2] T. Franke, E. Barbato, G. Bosia, et al. Technological and physics assessments on heating and current drive systems for DEMO. *Fusion Eng. Des.*, 96:468, 2015.

[3] M. Bacal and M. Wada. Negative hydrogen ion production mechanisms. *Appl. Phys. Rev.*, 2:021305, 2015.

[4] E. Speth, H. D. Falter, P. Franzen, et al. Overview of the RF source development programme at IPP Garching. *Nucl. Fusion*, 46:S220, 2006.

[5] C. Wimmer and U. Fantz. Dependence of the source performance on plasma parameters at the BATMAN test facility. *AIP Conf. Proc.*, 1655:040004, 2015.

[6] D. Wünderlich, S. Dietrich, and U. Fantz. Application of a collisional radiative model to atomic hydrogen for diagnostic purposes. *Journal of Quantitative Spectroscopy and Radiative Transfer*, 110:62, 2009.

[7] C. Wimmer. *Characteristics and Dynamics of the Boundary Layer in RF-driven Sources for Negative Hydrogen Ions*. PhD thesis, University of Augsburg - EPP, (Germany), 2014.

[8] R. Gutser, C. Wimmer, and U. Fantz. Work function measurements during plasma exposition at conditions relevant in negative ion sources for the ITER neutral beam injection. *Rev. Sci. Instrum.*, 82:023506, 2011.

[9] Y. I. Belchenko, G. I. Dimov, and V. G. Dudnikov. A powerful injector of neutrals with a surface-plasma source of negative ions. *Nucl. Fusion*, 14:113, 1974.

[10] R. Friedl and U. Fantz. Temperature dependence of the work function of cesiated materials under ion source conditions. *AIP Conf. Proc*, 1655:020004, 2015.

[11] B. S. Lee and M. Seidl. Surface production of H^- ions by hyperthermal hydrogen atoms. *Appl. Phys. Letters*, 61:2857, 1992.

[12] J. D. Isenberg, H. J. Kwon, and M. Seidl. Surface production of H^- ions by backscattering of H^+ and H_2^+ ions in the 3 - 50 eV ion energy range. *AIP Conf. Proc.*, 287:38, 1992.

[13] U. Fantz, P. Franzen, and D. Wünderlich. Development of negative hydrogen ion sources for fusion: Experiments and modelling. *Chem. Phys.*, 398:7, 2012.

[14] K. N. Leung, K. W. Ehlers, and R. V. Pyle. Effect of wall material on H^- production in a multicusp source. *Appl. Phys. Letters*, 47:227, 1985.

[15] O. Fukumasa and S. Saeki. Effect of wall material on negative ion production in a hydrogen plasma. *J. Phys. D: Appl. Phys.*, 20:237, 1987.

[16] W. G. Graham. Wall material and wall temperature effects on negative ion production in a hydrogen plasma. *J. Phys. D: Appl. Phys.*, 16:1907, 1983.

[17] T. Inoue, Y. Matsuda, Y. Ohara, et al. Effect of filament material and area on the extracted current from a volume H^- ion source. *Plasma Sources Sci. Technol.*, 1:75, 1992.

[18] C. F. A. van Os, P. W. van Amersfoort, and J. Los. Negative ion foramtion at a barium surface exposed to an intense positivehydrogen ion beam. *J. Appl. Phys.*, 64:3863, 1988.

[19] J. R. Hiskes and A. M. Karo. Recombination and dissociation of H_2^+ and H_3^+ ion on surfaces to form $H_2(\nu'')$: Negative ion formation on lowworkfunction surfaces. *J. Appl. Phys.*, 67:6621, 1990.

[20] P. Wurz, R. Schletti, and M. R. Aellig. Hydrogen and oxygen negative ion production by surface ionization using diamond surfaces. *Surf. Sci.*, 373:56, 1997.

[21] P. Kumar, A. Ahmad, C. Pardanaud, et al. Enhanced negative ion yields on diamond surfaces at elevated temperatures. *J. Phys. D: Appl. Phys.*, 44:372002, 2011.

[22] A. Ahmad, C. Pardanaud, M. Carrre, et al. Negative ion production on carbon materials in hydrogen plasma: Influence of the carbon hybridization state and the hydrogen content on H^- yield. *J. Phys. D: Appl. Phys.*, 47:085201, 2014.

[23] M. Bacal. Physics aspects of negative ion sources. *Nucl. Fusion*, 46:S250, 2006.

[24] M. Bacal, C. Michaut, L. I. Elizarov, et al. Basic processes of negative hydrogen ion production and destruction in sources and beams. *Rev. Sci. Instr.*, 67(3):1138, 1996.

[25] K. N. Leung, K. W. Ehlers, and M. Bacal. Extraction of volume-produced H^- ions from a multicusp source. *Rev. Sci. Instrum.*, 54:56, 1983.

[26] M. Bacal, A. A. Ivanon Jr., M. Glass-Maujean, et al. Contribution of wall material to the vibrational excitation and negative ion formation in hydrogen negative ion sources (invited). *Rev. Sci. Instr.*, 75:1699, 2004.

[27] A. G. Borisov and V. A. Esaulov. Negative ion formation in the scattering of atoms and ions from dielectric surfaces. *J. Phys.: Condens. Matter*, 12:R177, 2000.

[28] R. K. Janev. Destruction of negative ions near solid state surfaces. *Surf. Sci.*, 45:609, 1974.

[29] B. Rasser, J. N. M. van Wunnik, and J. Los. Theoretical model of the negative ionization of hydrogen on clean tungsten, cesiated tungsten and cesium surfaces at low energies. *Surf. Sci.*, 118:697, 1982.

[30] C. Goeden and G. Dollinger. Electron stimulated desorption on diamond (100) as negative hydrogen source. *Appl. Surf. Sci.*, 147:107, 1999.

[31] A. Hoffman, A. Laikhtman, S. Ustaze, et al. Dissociative electron attachment and dipolar dissociation of H^- electron stimulated desorption from hydrogen diamond films. *Phys. Rev. B.*, 63:045401, 2001.

[32] A. Ahmad, J. Dubois, T. Pasquet, et al. Negative-ion surface production in hydrogen plasmas: modeling of negative-ion energy distribution functions and comparison with experiments. *Plasma Sources Sci. Technol.*, 22:025006, 2013.

[33] C. I. Pakes, D. Hoxley, S. Rubanov, et al. Work function of hydrogen-terminated diamond surfaces under ion impact. *Surf. Sci.*, 601:5732, 2007.

[34] L. Diederich, O. M. Küttel, P. Aebi, et al. Electron affinity and work function of differently oriented and doped diamond surfaces determined by photoelectron spectroscopy. *Surf. Sci.*, 418:219, 1998.

[35] U. Kurutz and U. Fantz. Investigations on caesium-free alternatives for H^- formation at ion source relevant parameters. *AIP Conf. Proc.*, 1655:020005, 2015.

[36] O. Fukumasa and T. Iwasaki. Development of a double plasma type negative ion source. *AIP Conf. Proc*, 287:411, 1992.

[37] M. Bacal, G. W. Hamilton, A. M. Bruneteau, et al. Measurement of H^- density in plasma by photodetachment. *Rev. Sci. Instr.*, 50:719, 1979.

[38] F. F. Chen. Langmuir probes in RF plasma: surprising validity of OML theory. *Plasma Sources Sci. Technol.*, 18:035012, 2009.

[39] R. Rauner, U. Kurutz, and U. Fantz. Comparison of measured and modelled negative hydrogen ion densities at the ECR-discharge HOMER. *AIP Conf. Proc.*, 1655:020017, 2015.

[40] U. Fantz and B. Heger. Spectroscopic diagnostics of the vibrational population in the ground state of H_2 and D_2 molecules. *Plasma Phys. Control. Fusion*, 40:2023, 1998.

[41] U. Fantz, H. Falter, P. Franzen, et al. Spectroscopy - a powerful diagnostic tool in source development. *Nucl. Fusion*, 46:S297, 2006.

[42] B. Küppers et al. *Online reaction kinetics analysis, for chemistry in hydrogen plasmas*. Forschungszentrum Jülich GmbH, Jülich (Germany), 2015. [Online] Available: http://www.hydkin.de/.

[43] Alvatec GmbH, Austria. http://www.alvatec.com, 2015.

[44] D. Wünderlich, R. Gutser, and U. Fantz. PIC code for the plasma sheath in large caesiated RF sources for negative hydrogen ions. *Plasma Sources Sci. Technol.*, 18:045031, 2009.

[45] J. Yang, Z. Nie, X. Xi, et al. Emission ability of La-Sc-Mo cathode. *Appl. Surf. Sci.*, 229:51, 2004.

[46] M. A. Uijttewaal, G. A. de Wijs, and R. A.de Groot. Ab Initio Work Function and Surface Energy Anisotropy of LaB_6. *J. Phys. Chem. B*, 110:18459, 2006.

[47] Plansee Composite Materials GmbH, Germany. http://www.plansee.com/de/, 2001.

[48] Sindlhauser Materials GmbH, Germany. http://www.sindlhauser.de/, 2014.

[49] M. Schreck. University of Augsburg, Experimental Physics IV, (Germany) https://www.physik.uni-augsburg.de/lehrstuehle/exp4/, 2015.

[50] C. Gilles. Aix-Marseille Université - PIIM, (France), piim.univ-amu.fr, 2015.

[51] LSPM Laboratoire des Sciences des Procédés et des Matériaux (France). http://www-lpmtm.univ-paris13.fr/?lang=fr, 2015.

[52] B. Crowley. Culham Centre for Fusion Energy - CCFE, (UK) http://www.ccfe.ac.uk/, 2013.

[53] Heriot-Watt University: School of Engineering & Physical Sciences; Photonics & Quantum Sciences. http://www.hw.ac.uk/schools/engineering-physical-sciences/, 2015.

[54] DiaCCon GmbH, Germany. http://www.diaccon.de/de/, 2013.

[55] U. Fantz R. Friedl, U. Kurutz. Effeciency of Cs-free Materials for Negative ion Production in H_2 and D_2 Plasmas. to be published.

[56] R. Friedl and U. Fantz. Influence of cesium on the plasma parameters in front of the plasma grid in sources for negative hydrogen ions. *AIP Conf. Proc.*, 1515:255, 2013.